12 Physics of Biological Systems

Cornel Andreoli, Conrad Escher, Hans-Werner Fink, Michael Krüger,
Tatiana Latychevskaia, Hiroshi Okamoto, Gregory Stevens, Sandra Pascale Thomann.

in collaboration with:
Jevgeni Ermantraut, Clondiag Chip Technologies (Germany); Pierre Sudraud, Orsay Physics (France); Roger Morin, CNRS Marseille (France); John Miao, University of California at Los Angeles (USA); Dieter Pohl, University of Basel; Andreas Plückthun, Peter Lindner, Biochemistry Institute, University of Zurich; Bettina Böttcher, IMBL-European Institute for Molecular Biology, Heidelberg; Andre Geim, Centre for Mesoscience & Nanotechnology, University of Manchester; Werner Kühlbrandt, Max-Planck Institute of Biophysics, Frankfurt.

In the past year the group has been working on quantitative experiments to explore basic aspects of the energetic associated with a single DNA molecule in the liquid phase. A new quantum mechanical concept for reducing radiation damage in electron microscopy has been formulated and implemented. Progress has also been made towards our effort in trying to establish holography with low energy electrons as a new tool for structural determination of individual molecules. A dedicated Low Energy Electron Point Source microscope has been completed for these studies. Preliminary results indicate that it is possible to obtain holograms from unstained viruses. A solid electrolyte ion source has been invented in collaboration with a group at the University of Basel.

12.1 Studies of single DNA molecules in liquids [1]

The DNA molecule is a highly flexible biopolymer, capable of assuming a variety of configurations that are most likely strongly related to its functions in cells of living species. The packing of the DNA in the nucleus of the cell and the dynamics of the various enzymatic reactions require transitions between the configurations of the DNA. Thus, an insight into the free-energy landscape associated with the various configurations of the molecule is at the centre of a basic understanding of its physics and chemistry. Apart from the molecules biological function, the DNA as a biopolymer is also an important object to test and further develop the foundations of polymer physics. Following Kuhn's pioneering work a DNA molecule in a liquid is viewed as a chain of contour length L that is made up of individual elements of Kuhn-length A (often also referred to as persistence length) over which the molecule remains straight. If it costs little or even no energy to change the direction of all Kuhn-length elements in respect to each other, the molecule will assume a random coil equilibrium configuration at finite temperature. The random coil is thus the most likely configuration and its stability is believed to be strongly influenced by the entropy term as the main contribution towards the minimum of its free energy. In contrast, the straight configuration is the most unlikely one with the least number of possible different ways to realize it and thus associated with minimal entropy.

The question we addressed is how the transition from the straight to the random coil proceeds and whether or not this process is thermally activated, i.e. whether or not there is an activation barrier. The ability to observe individual molecules and to monitor their dynamics with video frequency time resolution, pioneered by Steven Chu, has become routine. How-

ever, establishing equilibrium conditions at different temperatures has never been achieved prior to our work, it is a pre-requisite to address the questions in relation to the molecules energetics.

Our experiments have been performed by using such fluorescence video microscopy as exemplified by the sequence of video frames shown in Fig. 12.1 where a λ-DNA molecule, straightened to itscontour length of 16 μm, undergoes a transition to the random coil. After the elapsed time associated with this particular transition, the molecule remains in a random coil configuration indicating that it indeed corresponds to the minimum of the free energy. The question mark in Fig. 12.1 refers to the issue of whether or not the transition from the straight to the random coil is associated with a barrier separating the two states. So far, no direct experimental evidence has established the existence of such a barrier.

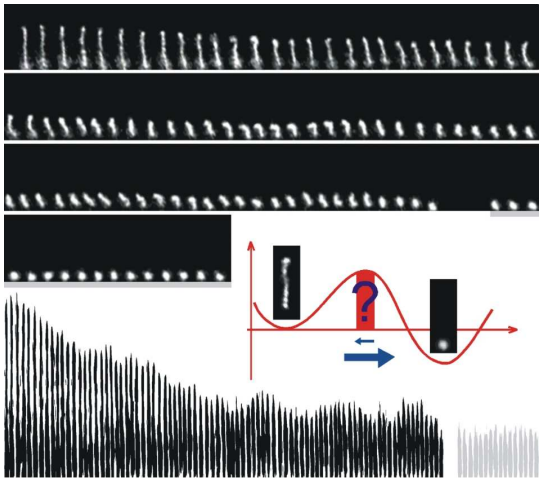

Figure 12.1:
Video fluorescence images taken of a single DNA molecule in the liquid are shown on top. After 85 frames the molecule has completed the transition from the straight to the random coil configuration at 15 ^{o}C. Thereafter, underlined in gray, the random coil remains. The bottom part repeats the raw data set shown on top, just with inverted color and stretched in vertical direction. The straight configuration with a maximum end-to-end separation corresponds to the contour length of about 16 μm for a λ-DNA molecule. It has been created here by employing an electric field after anchoring the bottom end of the molecule to the substrate. After the electric field has been switched off, equilibrium of the solvent is re-established and the DNA molecule evolves towards its equilibrium configuration, the random coil. The arrows in the inlet of the figure represent the very different probabilities of observing transitions between the two configurations and the ? is if there is a barrier separating the two configurations.

For such a task it is necessary to measure the transition time for a large number of events, such as the one illustrated in Fig. 12.1 to derive at a meaningful statistical ensemble for this process. To actually derive quantitative information directly from statistical experiments on the energetics of single molecules, the experimental set-up must be such that thermal equilibrium conditions, free from disturbances by the observation process, are guaranteed at different temperatures. Furthermore, routine methods for anchoring the 16 μm long and 2 nm thick molecules at one end have to be available: first, to provide a proper distance reference, second, to stretch the molecules and third, to be able to derive sufficient statistics and obtain quantitative energy values. This has been achieved in a close collaboration with Clondiag Chip Technologies[4] that provided us with state of the art molecular biology techniques for binding a molecule to a silicon oxide substrate. The experiments take place in a 10 μm thin water film in which stained λ-DNA of low concentration (5 pM) is embedded. The film is carefully sealed to avoid evaporation and associated erratic liquid flow and thus perturbation of the equilibrium conditions, essential for deriving quantitative free energy data, is suppressed.

[4]Clondiag Chip Technologies ®GmbH, Loebstedter Str.103-105, D-07749 Jena, Germany

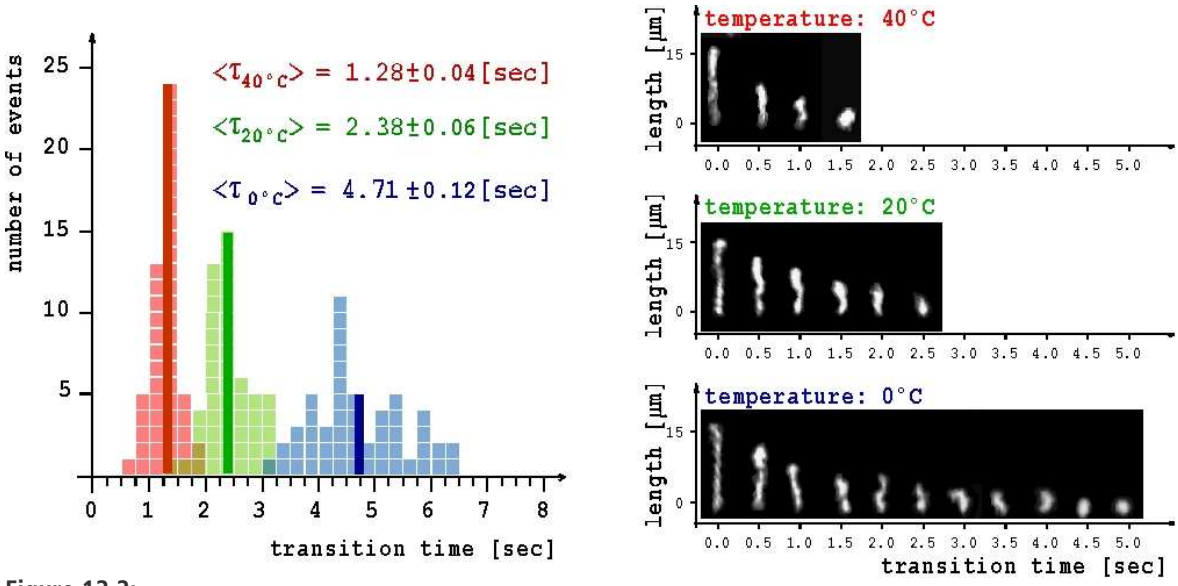

Figure 12.2:
Measurements of the transition time from the straight to the random coil DNA configuration. Right: Every 12th frame of the transition of a straight DNA towards the random coil is shown at 40, 20 and 0 ^{O}C. Left: The corresponding histograms of the distributions for the relaxation times and the average values are shown.

The epoxidated silicon oxide sample binds streptavidin, which in turn provides an anchor for the DNA molecules that are biotinylated at one end. For stretching the λ-DNA to its contour length, an electric field of typically 15 V/cm is employed. The field is provided by two gold lines shadow evaporated onto the substrate. The sample temperature is adjusted and controlled by a peltier stage underneath the sample and needs to be calibrated prior to the experiment. Once the temperature calibration is carried out, the experiments are performed in the following manner. A search is made for a single DNA molecule that is bound at one end to the substrate. This is done by applying an electric field and looking for a straightened molecule. The unbound molecules are just drifting through the field of view towards the electrode at positive potential. After having found a straight molecule, the electric field is switched to zero instantaneously by putting the two electrodes onto the same potential. Equilibrium of the liquid is thus provided immediately compared to the time scale that governs the molecular dynamics of the DNA. This can be verified by visual inspection of the stopping of the motion of unbound DNA molecules. Once this motion has stopped, it is evidence for thermodynamical equilibrium of the solvent in which the DNA then evolves towards the minimum of its free energy. With one particular molecule, typically 5 experiments of stretching and observing the progression towards the random coil configuration are performed. After having collected enough data, similar experiments are carried out at a different temperature. A total of 600 measurements at 12 different temperatures ranging from -5 to +50 ^{o}C were evaluated. In Fig. 12.2 the distribution of the observed relaxation times at three different temperatures are shown together with some sequences taken in the fluorescence video microscope.While the thermodynamically unlikely straight configuration is not observed under ordinary thermal conditions, it can be realized by applying an external electric field and, by switching off the field, the temporal evolution from the initial straight towards the configuration of minimal free energy can readily be measured. In the presence of an activation barrier, the lifetime of this straight configuration, respectively the transition time for the re-formation of the random coil can be written as:

$$\tau = \tau_0 e^{E_{rc}/kT} \tag{12.6}$$

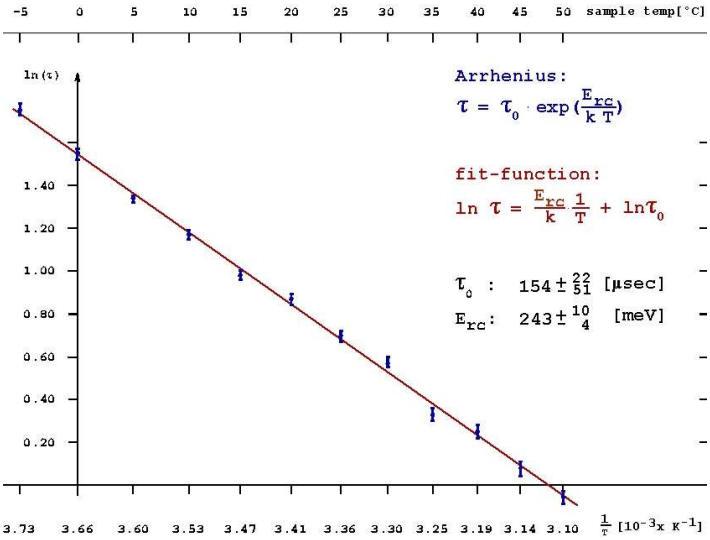

Figure 12.3:
Determination of the activation barrier height and pre-factor. According to Eq. 12.6, the data for the average transition times are represented in a semi-logarithmic plot. A least square fit to a linear dependence reveals the activation barrier E_{rc} and the pre-factor τ_0. The error bars reflect the statistical error of the average transition times (see also the raw data presented in Fig. 12.2).

where E_{rc} denotes the activation free energy barrier for the formation of the random coil. The pre-factor τ_0 is associated with the molecular fluctuations of the solvent. Both quantities are derived from an Arrhenius plot, as shown in Fig. 12.3. Apparently, the formation of the DNA random coil is associated with an activation barrier of the order of 0.25 eV. For a single DNA molecule, embedded in a liquid of constant volume, the Free Energy can be written as: $F = U - T \cdot S$; where U denotes the internal energy of the molecule and is determined by the binding energy between the atoms that make up the molecule; T is the absolute temperature and S the entropy given by the Boltzmann relation $S = k \cdot \ln W$.

The number of possible ways to generate a particular configuration of the DNA chain divided by all possible combinations to generate any configuration of the molecule defines the probability W for this particular configuration and determines its entropy value. Now, it is well known that short DNA molecules can be viewed as rigid rods. That implies that the stacking of the individual nucleotides is such that a straight configuration is energetically favourable and leads to a minimum of U. The response of a small DNA molecule to the Brownian agitation, i.e. the statistical motion of the surrounding solvent molecules, leads to translations and rotations of the rod within the liquid. The entropy plays a minor role and the free energy minimum is almost exclusively given by the internal energy U. For a longer molecule however, the stochastic momentum transfer by the solvent does no longer lead to purely translational and rotational motions of the entire molecule. A longer molecule has to develop kinks as a response to the Brownian agitation. This is purely an effect of size and associated increase of possible configurations. We have thus two extremes. A straight DNA chain corresponding to a minimum of the internal energy U and a small entropy contribution on one side. On the other side, a random coil configuration corresponding to an increased internal energy, which apparently is over-compensated by a large entropy term. The latter is due to the vast number of possible ways to form a random coil for a 16 μm long λ-DNA. At any experimentally accessible temperature between freezing the solvent and melting the molecule, the entropy term apparently dominates and defines the absolute minimum of the free energy.

[1] **Activation Barrier for the DNA Random Coil Formation**, Conrad Escher and Hans-Werner Fink, submitted to Phys.Rev.Lett..

12.2 A new quantum mechanical principle to reduce radiation damage in electron microscopy[1]

Radiation damage severely restricts our ability to study unstained biological specimens in electron microscopy. Reduction of the electron dose in order to keep the specimen intact results in poor image quality due to shot noise. As such, it is widely believed that the amount of extractable information from a single specimen is fundamentally limited. Here we show that this need not be the case when a structural hypothesis of a specimen is available. Quantum mechanical principles then allow the use of a very low electron dose to verify the hypothesis. To realize such a method, one has to control the electron wavefront. We propose to use micro-fabricated diffractive electron optical elements for this purpose. Despite the short electron wavelength, our experiments demonstrate that it is indeed possible to obtain a desired diffractive effect by fabricating such an element. Furthermore, numerical simulations combined with Bayesian statistical analysis were employed to quantitatively assess the strength of this new principle for structural biology. Quantum mechanics states that a measurement of an observable produces a deterministic outcome when a particle is in an eigenstate of the observable. Repetition of the measurement on particles prepared in an identical way quickly yields high confidence about the quantum state due to the absence of noise. The same principle can be applied to the case of electron microscopy, if the state of an electron after the scattering by a specimen is known. One can then design a corresponding electron-optical element that transforms the scattered wave, i.e., the object wave, to a converging spherical wave to produce a spot on an imaging screen. Therefore it is possible to be highly confident about a given structural model with a single electron only, because the chance of detecting an electron at a particular point on the screen by coincidence is low. By repeating the measurement, confidence about the structural model will increase rapidly. This is in a sharp contrast to conventional electron microscopy, which typically takes 10^8 electrons to generate an image with a fair signal to noise ratio. Transforming the object wave into a spherical converging wave can be done solely by linear optical elements (so-called matching filters), as has been studied in the optical image recognition context. Our diffractive element transmission function d is derived from a simple idea that if Ψ_0 is the object wave and Ψ_S is the convergent spherical wave, then d should be a solution of the following equation:

$$\Psi_S = d \cdot \Psi_0 \tag{12.7}$$

Thus, by illuminating the diffractive element d with an object wave Ψ_0, the spherical convergent wave Ψ_S is reconstructed behind the diffractive element, as shown in Fig. 12.4. Ideally, the transmission function of the diffractive element should provide both amplitude and phase modulation satisfying Eq.12.7. However, for micro-fabrication purpose, d must be described by a real and positive function. To overcome this obstacle,

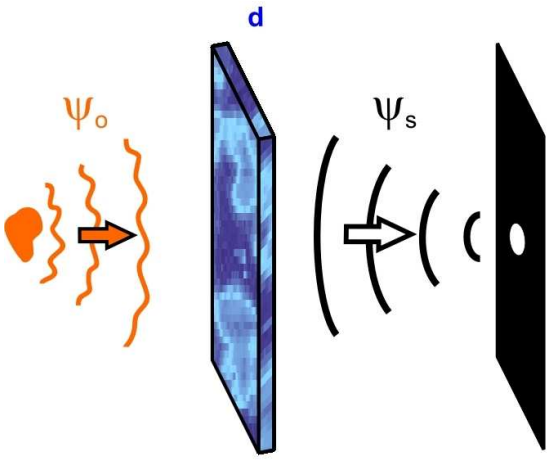

Figure 12.4:
The scheme to transform the object wave Ψ_0 from a specimen to a converging spherical wave Ψ_S by use of the diffractive element d. The structure of the diffractive element is simulated numerically in accordance with Eq. 12.8.

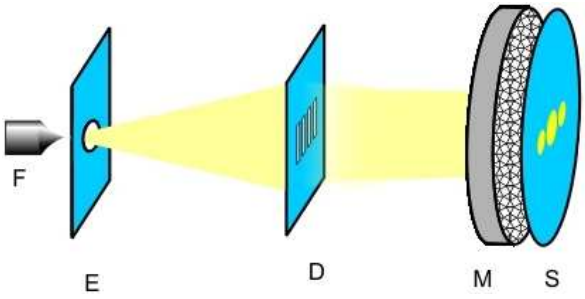

F: W(111) single crystal field emitter
E: carbon thin film extractor with a 1.2 μm diameter hole (Quantifoil R1.2/1.3) located 4 μm away from F.
D: diffraction grating located 360 μm away from E.
M: microchannel plate
S: phosphor screen

Figure 12.5:
Experimental setup. Diffractive elements were fabricated by an FIB apparatus (Orsay Physics), using a 30 keV, 2 pA Ga ion beam. They were milled in carbon support films with a nominal thickness of 12-20 nm (Quantifoil Micro Tools GmbH). Each hole was milled with a Ga ion dose of 4.7 fC, resulting in a diameter of approximately 20 nm. Because of the small diffraction angle, the image on the phosphor screen was magnified by an optical microscope, and subsequently recorded by a CCD camera.

our approach is to take the real part of the quotient

$$d = Re\{\Psi_S/\Psi_0\} + const \tag{12.8}$$

where the constant is added to ensure that d is always positive. To avoid division by zero, d was set to zero where the object wave intensity $|\Psi_0|^2$ is below a certain threshold. Thus, after the diffractive element, the emerging wave $d \cdot \Psi_0$ is proportional to the converging spherical wave Ψ_S and some additional terms.
Two remarks are in order. Firstly, in general we do not know *a priori* the exact place and orientation of a specimen, say a macromolecule. While small changes to the specimen position translates to the lateral displacements of the spot on the screen, the uncertainty of the specimen orientation poses a serious problem. Methods such as trapping the molecules in a well-defined manner may have to be employed. Secondly, if the structural hypothesis is incorrect, the experimenter will obtain an unexpected spot on the screen. However, this information could still be exploited by considering which alternative structural model is most likely to produce the particular spot obtained.
To realize the above scheme, we need freestanding diffractive elements that can be designed and fabricated at will. However, there have been no experimental demonstrations of engineered electron optics based on diffraction. To show that the above scheme can be implemented, we demonstrate electron diffraction by gratings, as well as rudimentary lens action by a diffractive element (see Fig. 12.5).
Figure 12.6 shows the fabricated slits of the gratings as imaged by low energy electron point source (LEEPS) microscopy. The recent wide availability of the focused ion beam (FIB) technology enabled us to fabricate such diffractive elements. The slit-to-slit distance was 100 nm. The array of 4 slits was approximated by a 4x4 array of 20 nm diameter holes with anisotropic hole-to-hole spacing, since it provided better mechanical strength. Since the characteristic feature size of the fabricated structures exceeds typical low energy electron wavelengths by a factor of several hundreds, we must stay in the paraxial optical regime. The high spatial coherence of the electron beam from the sharp field emitter guarantees the electron wave over the whole diffraction grating to be coherent. The relatively large distance of 360 μm between the electron source and the diffraction element ensured that, despite divergence from the point source, the angular spread of the incoming beam was smaller than the expected diffraction angle. The distance between the electron source and the screen was 100 mm, implying that our concept can be implemented without resorting to large instrumentation. Figure 12.7 shows a resultant image of the diffraction experiment performed with

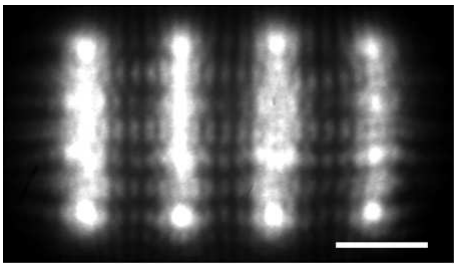

Figure 12.6:
LEEPS image of a diffraction grating taken with 69 eV electrons. Patterns other than the shadow images of the actual holes are due to Fresnel diffraction. Scale bar: 100 nm.

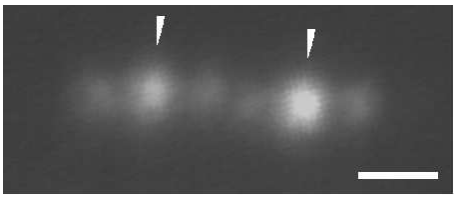

Figure 12.7:
A diffraction pattern produced by two diffraction gratings. Diffraction patterns of each of the gratings exhibits zeroth order spots (indicated by arrows) in between two first order diffraction spots. The electron energy was 149 eV. Scale bar: 3 mrad.

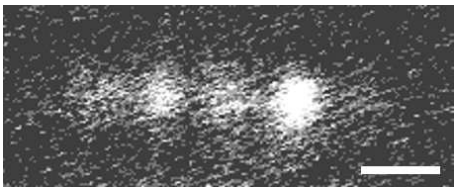

Figure 12.8:
When the electron energy was lowered to 90 eV, the two first order diffraction spots merged. Scale bar: 3 mrad.

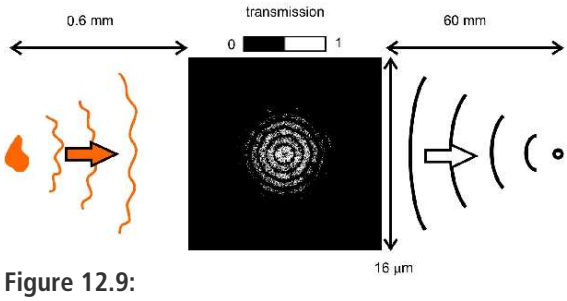

Figure 12.9:
An illustration of the experimental setup used in the simulations. The molecule is assumed to be in a vacuum. The incident electron beam diameter is slightly larger than the molecule. The diffractive element transmission map corresponds to the simulated diffractive element for ribosome 70S using 15 keV electrons.

149 eV electrons. The first order diffraction spots are clearly visible at an angle of 1.9 mrad from the zeroth order spots. This is close to the expected angle of 1.7 mrad derived from the measurement of the slit geometry, taking the electron beam divergence and the finite slit width into account. Furthermore, this angle changed consistently with the electron wavelength, which was varied from 0.073 nm to 0.13 nm, thus confirming that these spots are indeed due to diffraction. Figure 12.8 shows a rudimentary lens action, where the two diffraction spots merged into one when the electron energy was lowered to 90 eV.

To find out how many electrons are needed to identify the correct object with our scheme we set a moderate goal of recognizing the orientation of 70S ribosome[4] out of two possible orientations: a 'right' orientation and a 'wrong' orientation, which differ by 90 degrees. Our hypothesis is that ribosome is in the 'right' orientation, and we compute how many electrons are needed to verify the hypothesis. Figure 12.9 shows the experimental scheme, that was used in our simulations. Two distinct situations were considered. In the first case, the ribosome was treated as an amplitude and phase object, which refers to experiments in the low kinetic energy regime up to about 15 keV. In the second case, the ribosome was modeled as a pure phase object referring to the conventional electron microscopy regime of 100 keV. The diffractive element structures were simulated according to Eq.12.8 and converted to binary format, so that the structures are either fully transparent or opaque, with pixel sizes of 40 nm and 20 nm for 15 keV and 100 keV electrons, respectively. The random electrons arrival positions, obeying a probability distribution given by the intensity on the screen when the ribosome is in the 'right' orientation, were generated by a Monte Carlo method. In both energy cases, when the object is in the 'right' orientation, after a significant amount of electrons have been detected, a spot can be clearly seen on the screen and no special statistical analysis is required. To obtain high confidence of the object identifi-

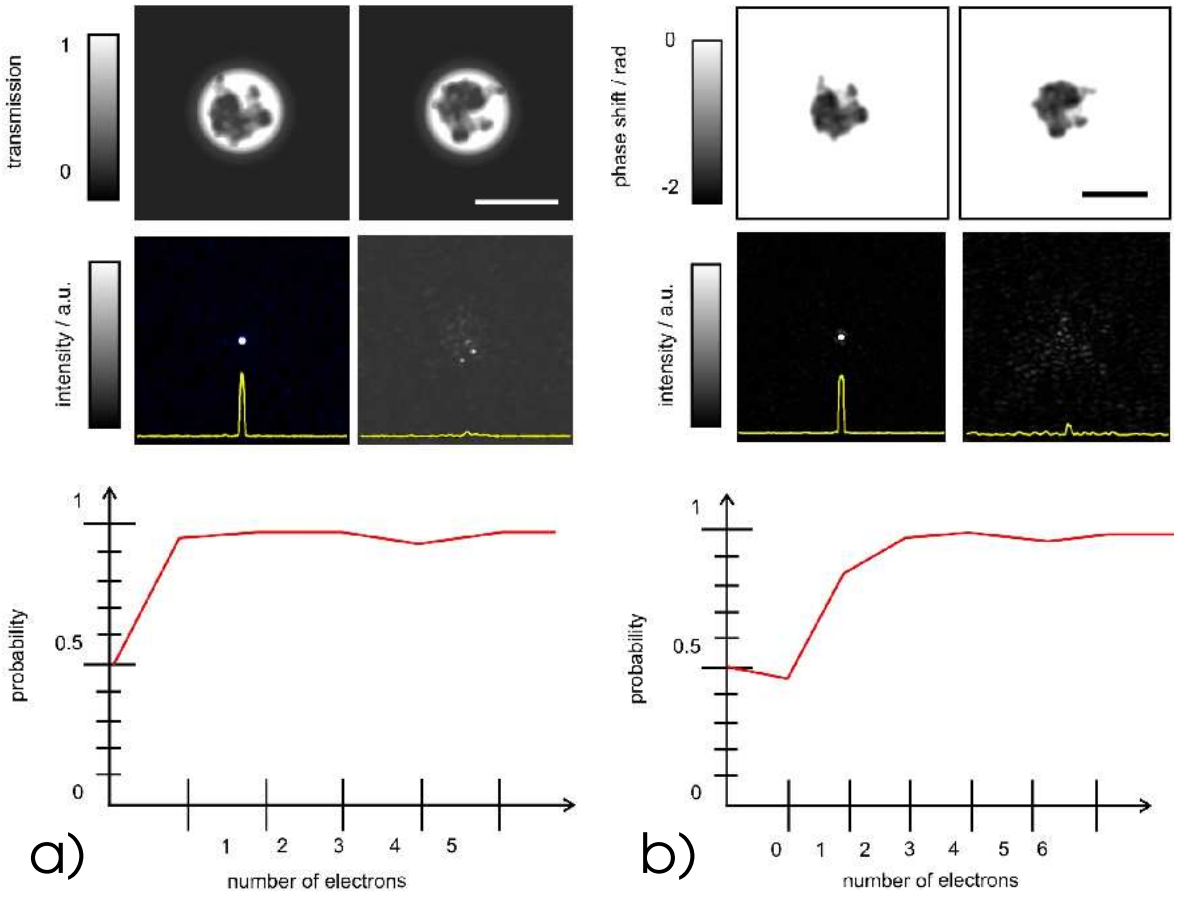

Figure 12.10:
The ribosome S70 at different electron energies can be considered as an amplitude and phase object (at 15 keV, a) or as a pure phase object (at 100 keV, b). The upper pictures show the transmission or phase shifts of the specimens. Scale bar: 20 nm. The pictures in the middle row show the intensity distribution on the screen. The yellow curves are the profiles of the intensity in the middle of the screen. A single spot is observed on the screen when the object is in the 'right' orientation (left picture) and scattered spots when the ribosome is rotated by 90^o (right picture). The graphs in the lower row show the confidence level for the hypothesis about the molecular orientation as a function of the number of electrons detected. The absorption coefficient was calculated using electron inelastic mean free path data. The phase shift was calculated using a known inner potential of the amorphous carbon, which was properly scaled by the equivalent effective carbon density.

cation with a few electrons only, Bayesian statistical analysis was applied to each detected electron. Our numerical experiments have shown that 4±3 electrons are needed at both, 15 keV and 100 keV, to identify the correct object with 95% confidence, see Fig. 12.10a and Fig. 12.10b. However, the absorption by the diffractive element must be taken into account, which changes the number of required electrons to 49±37 electrons at 15 keV and 607±438 electrons at 100 keV. There is considerable leeway for reducing the dose further to a few electrons by placing the diffractive element in between a convergent wave electron source and the specimen. In this case, use of an off-axis configuration would further eliminate irradiation of the specimen by unnecessary electron waves that are due to the zeroth order diffraction.

Apart from practical considerations, a question of fundamental interest is whether or not the above method represents the theoretical limit of radiation damage reduction. As a final remark, we briefly sketch a thought experiment showing that repeated use of an electron could in principle further increase the amount of obtainable structural information for a given radiation damage. Biological samples generally behave as weak phase objects at high electron energies, requiring a high dose especially when we want to discriminate between two similar hypotheses. A radical way to deal with this situation would be to collide an electron wavepacket n times with the specimen, refocusing the electron wave each time. This is essentially equivalent to having a stronger phase object. An incorrect structural hypothesis leads to the failure of subsequent transformation to the spherical wave by the diffractive element, which results in the 'error component' wave with an amplitude proportional to n. This means that the probability of detecting electrons outside the expected region is proportional to n^2, whereas the specimen damage grows as n. Thus, the hypothesis discrimination ability scales as n. This argument indicates that in principle there is room for further reducing radiation damage.

[1] **Controlling radiation damage in electron microscopy**, Hiroshi Okamoto, Tatiana Latychevskaia and Hans-Werner Fink, submitted to Phys.Rev.Lett..

12.3 Structure of individual Bio molecules

Gregory Stevens and Michael Krüger

in collaboration with: Andreas Plückthun and Peter Lindner, Biochemistry Institute

The aim of this project is to develop tools and methods to obtain structural information about individual biological macromolecules using coherent low-energy electrons. Novel methods have been developed to prepare specimens of individual macromolecules and the first low-energy electron holograms have been obtained. These investigations began with a filamentous phage called M13, which is attached to a carbon support film so that individual macromolecules are suspended over holes in the film. We are also using tobacco mosaic virus, because it has a 2.3 nm repeating surface feature that can be used to refine our imaging methods.
Since April 2004, we have designed and built, with the excellent support of our mechanical workshop a bio-LEEPS microscope for making low-energy electron holograms of individual biological molecules. The special requirements of this microscope include ease of use and rapid replacement of the specimen and electron source. Figure 12.11 shows the main parts of the microscope. A 'positioner' to remotely move the electron source in relation to the specimen has been made using three Attocubes, which are a new type of linear motor that utilize a piezo-electric crystal stack in a 'slip-stick' configuration to move macroscopic distances in steps of 50 nm. The positioner is shown with a vibration isolator that prevents vibrations in electrical wiring, and from acoustic noise, from disrupting the relative positions of the electron source and specimen.

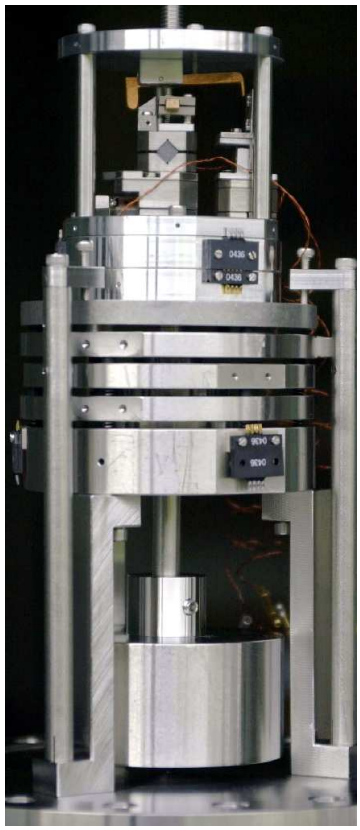

Figure 12.11:
Bio-LEEPS microscope 'positioner' with three Attocube linear motors to move the electron source in relation to the specimen, on a vibration-isolation stack.

Figure 12.12 shows a preliminary low-energy electron hologram of M13 phage suspended across a hole in a carbon film. This sample was prepared in a purpose-built freeze-drying chamber, which allows removal of water from the specimen in a way that minimizes rearrangement of individual macromolecules on a substrate film. Screen defects and an image of a deflecting screen were removed from the hologram by subtracting a background image of the detector screen. Future efforts will be directed to obtaining higher order fringes in the holograms. This may be achieved by improving the stability and coherence of the electron source and the sensitivity of the phosphor detector screen.
Figure 12.13 shows a conventional cryo-transmission electron microscope (cryo-TEM) image of unstained freeze-dried tobacco mosaic virus and M13 phage suspended across a hole in a carbon film. These images were taken using a low dose imaging method to minimize radiation damage. The ability to image unsupported macromolecules will allow comparison of images obtained in the cryo-TEM with bio-LEEPS images.
Further experiments will address whether the macromolecules are rearranged and/or undergo visible conformational changes during freeze-drying by periodically examining the specimen during freeze-drying in the cryo-TEM. In other experiments, we will label the phage with gold crystals of a known size in order to provide a calibration object for reconstructing the object from the hologram.

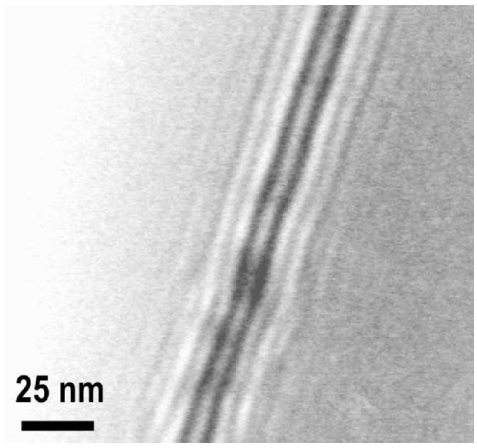

Figure 12.12:
100 eV in-line electron hologram of M13 phage obtained with the bio-LEEPS microscope.

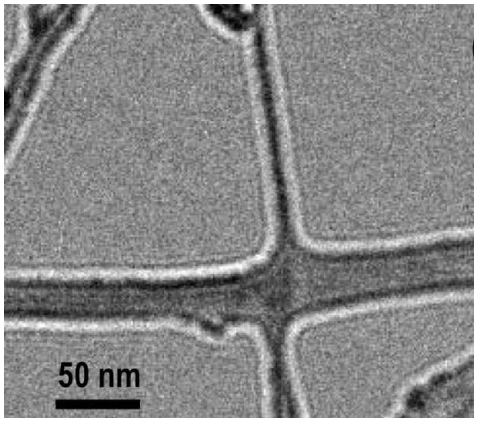

Figure 12.13:
200 keV cryo-transmission electron microscope image of freeze-dried tobacco mosaic virus and M13 phage suspended across holes in holey carbon film. We gratefully acknowledge the Max Planck Institutes of Biophysics for the use of their facilities in making this image.

12.4 A solid electrolyte ion source[1]

A cold source for silver ions has been invented. Source size and brightness are two major properties that allow the use of ions combined with electrostatic lenses to derive at focused ion beams. The current state of the art is represented by gallium ion beams of sizes as small as 5 nm that originate from a liquid metal source. Since these tools are ideally suited for structuring devices on the nanometer-scale, their importance shall increase in the future. Here we present a novel ion source, which is based on mobile silver ions in an electrolyte that are emitted at a well-defined source area of sub-micron dimension and accelerated by an electric field into a vacuum environment. To achieve this, amorphous $(AgJ)(AgPO_3)$ has been shaped into the form of a tip. By using field ion microscopy techniques the emission of silver ions has been investigated and characterized. It turns out that this first cold metal ion source exhibits unique properties with promising perspectives in scientific and technological applications.
There are various possibilities of creating ions, ranging from plasma sources to employing field ionisation to create ions from neutral gas atoms. However, the use of electrostatic

lenses for obtaining focused ion beams in the nanometer-sized regime requires ion sources of high brightness, which excludes conventional plasma sources and gas field ionisation sources. Thus, in view of source size and current per unit emission angle, today's technology is limited to the application of liquid metal ion sources in combination with ion-optical devices to reach focused beams of gallium ions as small as 5 nm.
We have invented a novel type of ion source, namely here the first cold and bright silver ion source which physics of operation is quite different from liquid metal sources. Ions from a conducting solid electrolyte are emitted into the vacuum at a constriction that is provided by geometry. In contrast to the ionisation of neutral species by an electric field, the ionic state is already present in the solid. This implies that at the location of ion emission, an equally high electron current into the source, as is unavoidable in the field ionisation sources and believed to be responsible for the broad energy spread of the ions, is not present in the silver ion source presented here.
The main design criteria for this novel source is associated with shaping the solid electrolyte (AgJ)($AgPO_3$) in such a way as to limit an electric field to a small source size region at which the Ag+ ions can overcome the binding to the solid and get transferred into the vacuum. Two basic designs have been tried and successfully been tested in a Field Ion Microscope.

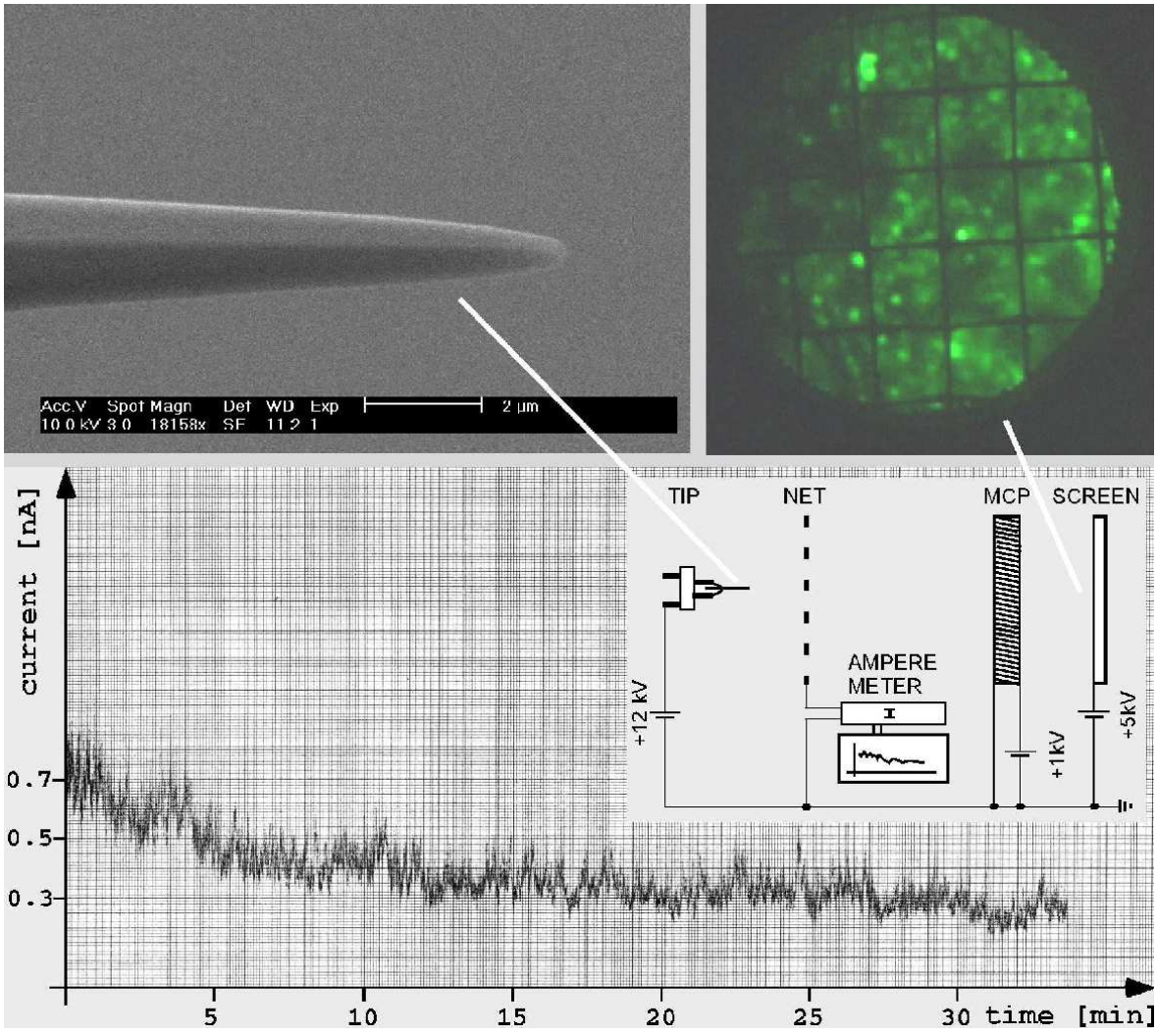

Figure 12.14:
Silver ion emission from an AgJ tip as observed in the Field Ion Microscope; see text for explanation.

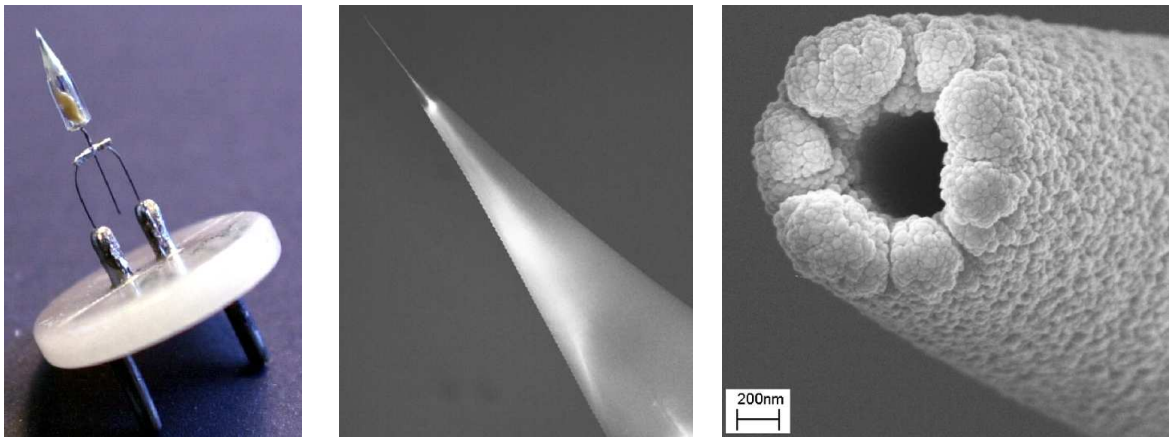

Figure 12.15:
Capillary Silver Ion source shown with increasing magnification. A glass capillary is filled with the conducting electrolyte. The ion emission occurs at the very end of the capillary. The opening of the capillary and with this the emission area can be further reduced by prior depositing silver onto the glass structure. An SEM image of such a capillary opening is shown at the right part of the figure.

Design 1 follows the concept of shaping the electrolyte into the form of a tip by various means of using the molten electrolyte and attaching it to a silver reservoir. It is shown in Fig. 12.14.

The (AgI)($AgPO_3$) material wets a silver wire and is formed into a tip (see SEM image in the upper left of Fig. 12.14) and mounted as a source in the Field Ion Microscope. To measure the emission current out of the tip and simultaneously observe the emission pattern with video frequency on the screen, a grid is assembled between tip and MCP. An Ampere-meter is connected to the grid to measure the current from grid to ground. The cross section of the grid covers about 5% of the beam current and therefore the measured values need to be multiplied by a factor of 20 to determine the total emission current of Ag^+ ions. Design 2 follows the idea of providing a form for the electrolyte to accommodate to, a mantle that provides the appropriate geometry and definition of the source area (see Fig. 12.15). This has been accomplished by filling a fine glass capillary with the molten electrolyte material and then quenching it to its solid amorphous state.

[1] **High brightness solid state ion generator, its use, and method for making such generator**,
Patent filed in March 2005. Invented by: Conrad Escher, Sandra Thomann, Cornel Andreoli and Hans-Werner Fink (University of Zurich), Julien Toquant and Dieter Pohl (University of Basel).